6058 *Inorg. Chem.* **2010**, *49*, 6058–6065
DOI: 10.1021/ic100598v

Inorganic Chemistry
Article

Crystal Structure and Phase Transitions in Sr_3WO_6

Graham King,*,† Artem M. Abakumov,‡,§ J. Hadermann,‡ Anastasiya M. Alekseeva,§ Marina G. Rozova,§ Tyche Perkisas,‡ Patrick M. Woodward,† Gustaaf Van Tendeloo,‡ and Evgeny V. Antipov§

†*Department of Chemistry, The Ohio State University, 100 West 18th Avenue, Columbus, Ohio 43210-1185,*
‡*EMAT, University of Antwerp, Groenenborgerlaan 171, B-2020 Antwerp, Belgium, and*
§*Department of Chemistry, Moscow State University, Moscow 119991, Russia*

Received March 30, 2010

The crystal structures of the β and γ polymorphs of Sr_3WO_6 and the $\gamma \leftrightarrow \beta$ phase transition have been investigated using electron diffraction, synchrotron X-ray powder diffraction, and neutron powder diffraction. The γ-Sr_3WO_6 polymorph is stable above $T_c \approx 470$ K and adopts a monoclinically distorted double perovskite $A_2BB'O_6 = Sr_2SrWO_6$ structure (space group *Cc*, $a = 10.2363(1)$ Å, $b = 17.9007(1)$ Å, $c = 11.9717(1)$ Å, $\beta = 125.585(1)^\circ$ at $T = 1373$ K, $Z = 12$, corresponding to $\mathbf{a} = \mathbf{a}_p + 1/2\mathbf{b}_p - 1/2\mathbf{c}_p$, $\mathbf{b} = 3/2\mathbf{b}_p + 3/2\mathbf{c}_p$, $\mathbf{c} = -\mathbf{b}_p + \mathbf{c}_p$, $\mathbf{a}_p$,$\mathbf{b}_p$, $\mathbf{c}_p$, lattice vectors of the parent $Fm\bar{3}m$ double perovskite structure). Upon cooling it undergoes a continuous phase transition into the triclinically distorted β-Sr_3WO_6 phase (space group *C*1, $a = 10.09497(3)$ Å, $b = 17.64748(5)$ Å, $c = 11.81400(3)$ Å, $\alpha = 89.5470(2)^\circ$, $\beta = 125.4529(2)^\circ$, $\gamma = 90.2889(2)^\circ$ at $T = 300$ K). Both crystal structures of Sr_3WO_6 belong to a family of double perovskites with broken corner sharing connectivity of the octahedral framework. A remarkable feature of the γ-Sr_3WO_6 structure is a non-cooperative rotation of the WO_6 octahedra. One third of the WO_6 octahedra are rotated by $\sim 45^\circ$ about either the b_p or the c_p axis of the parent double perovskite structure. As a result, the WO_6 octahedra do not share corners but instead share edges with the coordination polyhedra of the Sr cations at the *B* positions increasing their coordination number from 6 to 7 or 8. The crystal structure of the β-phase is very close to the structure of the γ-phase; decreasing symmetry upon the $\gamma \rightarrow \beta$ transformation occurs because of unequal octahedral rotation angles about the $\mathbf{b}_p$ and $\mathbf{c}_p$ axes and increasing distortions of the WO_6 octahedra.

1. Introduction

The well-known double perovskite ($A_2BB'O_6$) and elpasolite ($A_2BB'F_6$) structures can be derived from the simple ABX_3 perovskite structure by the introduction of two *B*-site cations arranged in a rock-salt fashion. The ideal structures are cubic with $Fm\bar{3}m$ symmetry and a lattice parameter which is twice that of the basic perovskite. While there are a number of double perovskites with cubic symmetry, most compounds undergo distortions from the ideal structure. The most common distortions are octahedral tilting distortions, which occur when the *A*-site cation is too small to fill the cuboctahedral cavity within the $BB'X_6$ framework. When this is the case the BX_6 and $B'X_6$ octahedra will rotate as nearly rigid units, thereby maintaining the $B-X$ and $B'-X$ distances while allowing for shorter $A-X$ distances.

It is generally assumed that the possible modes of octahedral tilting are limited by the fact that the corner sharing connectivity of the BX_3 (or $BB'X_6$) network must be maintained. On the basis of this assumption it is possible to enumerate all the space groups and the corresponding lattice vectors that can arise from the various combinations of in-phase and out-of-phase octahedral tilting.[1−3] This approach has also been applied to double perovskites with a rock salt type ordering of the *B* and *B*′ cations.[4−6] While almost all known perovskites obey this restriction, in the past few years there have been reports of compounds where the corner sharing connectivity is not maintained. This only occurs when there is a very large difference in ionic radius (ΔIR) between the *B* and *B*′ cations and a small tolerance factor. The required size mismatch was evaluated as $\Delta IR = 0.76-0.85$ Å for the $A_2BB'F_6$ elpasolites and $\Delta IR = 0.50-0.66$ Å for the $A_2BB'O_6$ double perovskites.[7] When this is the case the smaller *B*′ cations will retain octahedral coordination but the rotations of the $B'O_6$ octahedra are no longer cooperative, which allows the larger *B* cations to obtain coordination numbers greater

*To whom correspondence should be addressed. E-mail: gking@chemistry.ohio-state.edu.

(1) Howard, C. J.; Stokes, H. T. *Acta Crystallogr.* **1998**, *B54*, 782–789.
(2) Woodward, P. M. *Acta Crystallogr.* **1997**, *B53*, 32–43.
(3) Stokes, H. T.; Kisi, E. H.; Hatch, D. M.; Howard, C. J. *Acta Crystallogr.* **2002**, *B58*, 934–938.
(4) Howard, C. J.; Kennedy, B. J.; Woodward, P. M. *Acta Crystallogr.* **2003**, *B59*, 463–471.
(5) Lufaso, M. W.; Barnes, P. W.; Woodward, P. M. *Acta Crystallogr.* **2006**, *B62*, 397–410.
(6) Flerov, I .N.; Gorev, M. V.; Aleksandrov, K. S.; Tressaud, A.; Grannec, J.; Couzi, M. *Mat. Sci. Eng.* **1998**, *R24*, 81–151.
(7) Abakumov, A. M.; King, G.; Laurinavichute, V. K.; Rozova, M. G.; Woodward, P. M.; Antipov, E. V. *Inorg. Chem.* **2009**, *48*, 9336–9344.

 Published on Web 06/09/2010

than six. By removing the restriction of corner sharing connectivity it is possible to obtain structure types that have not been identified before.

The simplest examples of compounds with broken corner sharing connectivity of the octahedral framework are the elpasolite-type fluorides Rb_2KCrF_6 and Rb_2KGaF_6.[8] At room temperature these compounds have the ideal cubic $Fm\bar{3}m$ structure. At low temperature they undergo a transition to tetragonal symmetry which involves a rotation of 1/5 of the CrF_6 or GaF_6 octahedra by ~45° about the *c*-axis while the other octahedra remain in the same orientation as in the room temperature cubic structure. This allows 4/5 of the larger K ions to obtain a seven coordinate distorted pentagonal bipyramidal geometry while the remaining 1/5 of the K atoms retain octahedral coordination. A similar but more complex pattern of non-cooperative octahedral tilting has been discovered in α-K_3AlF_6.[7,9] In this compound 2/5 of the AlF_6 octahedra are rotated by ~45°. As in the Rb_2KMF_6 compounds, 1/5 of the AlF_6 octahedra are rotated by ~45° about the *c*-axis, but additionally 1/10 of the AlF_6 octahedra are rotated by ~45° about the *b*-axis and 1/10 are rotated ~45° about the *a*-axis. This results in 2/5 of the *B*-site K ions becoming 7-coordinated and the other 3/5 becoming 8-coordinated. A similar structure is suspected for $K_3MoO_3F_3$.[10,11]

Although the majority of structures with broken corner sharing connectivity of the octahedral framework are fluorides or oxyfluorides, nothing prevents mixed oxides from adopting such a structure. Until now, only the *A*-site deficient perovskites $A_7\square B_4B'_4O_{24}$ ($A = B$ = Ca, Sr, B' = Re, Os, □ = vacancy at the *A*-sublattice) are known where a rotation of 50% of the small $B'O_6$ octahedra by ~45° raises the coordination number of all *B* cations to 8.[12−14] However, there are other mixed oxides apparently based on the double perovskite structure that fall within the size mismatch of ΔIR = 0.50−0.66 Å. Sr_3WO_6 (Sr_2SrWO_6) is one such compound because of the large size mismatch between Sr^{2+} and W^{6+} (ΔIR = 0.58 Å).

It has been known for several decades that the cation lattice of Sr_3WO_6 is based on the double perovskite structure, but the nature of the anion lattice remains unknown.[15,16] Because of the high complexity of the structure no structural determination has been performed. It has also been observed that Sr_3WO_6 passes through a number of phase transitions upon heating.[17] Above 1320−1373 K Sr_3WO_6 adopts the cubic $Fm\bar{3}m$ structure,[16−20] but at room temperature a triclinic distortion of the cubic subcell has been reported.[20]

We have hypothesized that non-cooperative octahedral rotations could be responsible for the structural complexity of the Sr_3WO_6 polymorphs below the transition temperature from the cubic phase. Here we report a detailed structural analysis of Sr_3WO_6 including the complete structure solution of two ordered polymorphs stable in the 300−1373 K range using a combination of electron diffraction, neutron powder diffraction, and synchrotron X-ray powder diffraction. The structures can be described as variants of the double perovskite where 1/3 of the WO_6 octahedra are rotated by ~45° about double perovskite subcell axes.

2. Experimental Section

The Sr_3WO_6 samples were synthesized using conventional ceramic methods starting from $SrCO_3$ and WO_3. The initial materials were ground together under acetone and pressed into pellets. The sample for synchrotron powder X-ray diffraction was prepared by heating of the pellet in air at 1523 K for 100 h. The large batch for the powder neutron diffraction study was prepared by heating for 8 h at 1273 K. All samples were furnace cooled. The quality of the samples was monitored using powder X-ray diffraction with a Huber G670 Guinier diffractometer ($CuK_{\alpha 1}$ radiation, curved Ge monochromator, transmission mode, image plate).

The samples for the electron diffraction investigation were prepared by crushing the powder sample in ethanol and depositing it on a holey carbon grid. Selected area electron diffraction (ED) patterns were recorded using Philips CM20 and Tecnai G2 microscopes equipped with heating holders.

Synchrotron X-ray powder diffraction (SXPD) data were collected on beamline ID31 at the ESRF, Grenoble (λ = 0.39998 Å). The data were collected by eight linear position-sensitive detectors in the angular range $2\theta = 1-40°$. The powder sample was placed into a quartz capillary with the internal diameter of 0.5 mm. To achieve good statistics and to avoid preferred orientation, the capillary was rotated during the experiment. The sample was heated above room temperature (RT) with a hot-air blower. Long scans were collected at 300, 400, 623, 1023, and 1173 K. A number of short scans were also collected to monitor the phase transition. Time-of-flight neutron powder diffraction (NPD) data were collected at the HRPD beamline at the ISIS facility of the Rutherford Appleton Laboratory. Patterns were collected at 300, 498, 798, 898, and 1373 K.

The structure solution using a Monte Carlo based global optimization was undertaken using the FOX program.[21] The software JANA2006[22] was used for refinement of the β phase while the Topas Academic[23] program package was used for the structure determination and Rietveld refinement of the γ phase.

3. Results and Discussion

3.1. Unit Cell Determination and Phase Transitions. The SXPD patterns taken at 300 and 1173 K (Figure 1) demonstrate that Sr_3WO_6 is a member of the double perovskite family. The most intense reflections in these patterns correspond to a face centered pseudo-cubic

(8) Zuniga, F. J.; Tressaud, A.; Darriet, J. *J. Solid State Chem.* **2006**, *179*, 3607–3614.
(9) Abakumov, A. M.; Rossell, M. D.; Alekseeva, A. M.; Vassiliev, S. Y.; Mudrezova, S. N.; Van Tendeloo, G.; Antipov, E. V. *J. Solid State Chem.* **2006**, *179*, 421–428.
(10) Brink, F. J.; Withers, R. L.; Friese, K.; Madariaga, G.; Noren, L. *J. Solid State Chem.* **2002**, *163*, 267–274.
(11) Withers, R. L.; Welberry, T. R.; Brink, F. J.; Noren, L. *J. Solid State Chem.* **2003**, *170*, 211–220.
(12) Jeitschko, W.; Moens, H. A.; Rodewald, U. C.; Möller, M. H. *Z. Naturforsch.* **1998**, *53*, 31–36.
(13) Bramnik, K. G.; Miehe, G.; Ehrenberg, H.; Fuess, H.; Abakumov, A. M.; Shpanchenko, R. V.; Pomjakushin, V.Yu.; Balagurov, A. M. *J. Solid State Chem.* **2000**, *149*, 49–55.
(14) Tomaszewska, A.; Müller-Buschbaum, H. *Z. Anorg. Allg. Chem.* **1993**, *619*, 1738–1742.
(15) Kroger, F. A. *Nature* **1947**, *159*, 674–5.
(16) Steward, E. G.; Rooksby, H. P. *Acta Crystallogr.* **1951**, *4*, 503–507.
(17) Drache, M.; Ravez, J.; Hagenmuller, P. *Solid State Commun.* **1981**, *37*, 139–143.
(18) Chang, L. L. Y.; Scroger, M. G.; Phillips, B. *J. Am. Ceram. Soc.* **1966**, *49*, 385–390.
(19) Chang, L. L. Y.; Phillips, B. *J. Am. Ceram. Soc.* **1967**, *50*, 434–435.
(20) Kovba, L. M.; Lykova, L. N.; Shevchenko, N. N. *Zh. Neorg. Khim.* **1973**, *18*, 1991–1992.
(21) Favre-Nicolin, V.; Černy, R. *J. Appl. Crystallogr.* **2002**, *35*, 734–743.
(22) Petricek, V.; Dusek, M. *JANA2000: Programs for Modulated and Composite Crystals*; Institute of Physics: Praha, Czech Republic, 2000.
(23) *Topas Academic, General Profile and Structure Analysis Software for Powder Diffraction Data*; Bruker AXS: Karlsruhe, Germany, 2004.

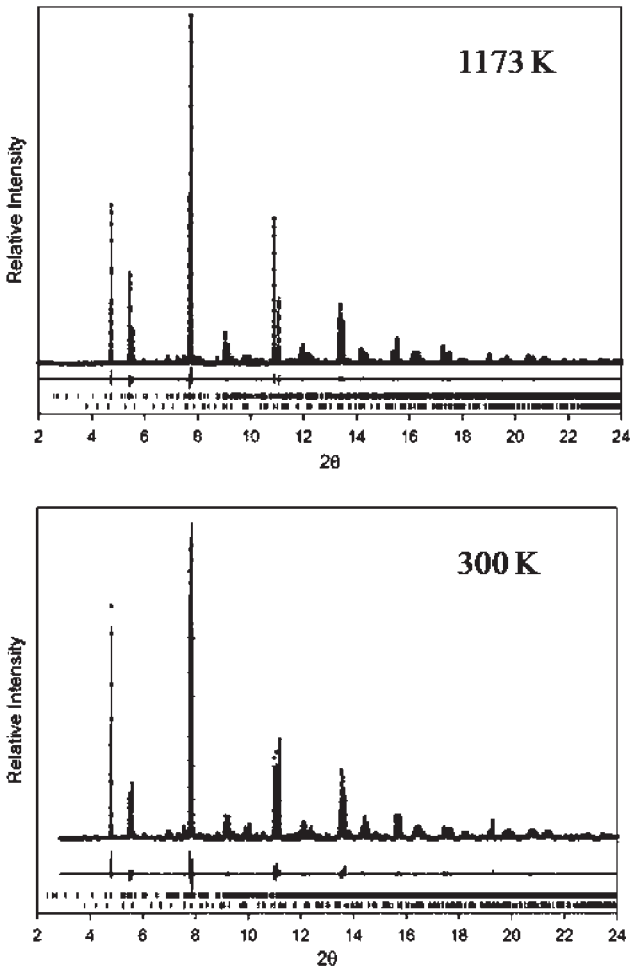

Figure 1. SXPD patterns at 300 and 1173 K showing the observed (circles), calculated (solid line), and difference (beneath) after Rietveld refinement. The upper tick marks are the *hkl* positions for the Sr_3WO_6 phase, and the lower tick marks are the *hkl* positions for the Sr_2WO_5 impurity phase.

subcell with $a = 2a_p \approx 8.3$ Å. (a_p is the parameter of the simple perovskite unit cell). Our investigation and the literature data suggest that Sr_3WO_6 has four polymorphs which will be further denoted as α, β, γ, and δ on going from low to high temperature.

The δ-Sr_3WO_6 polymorph possesses the cubic $Fm\bar{3}m$ structure with a $2a_p \times 2a_p \times 2a_p$ unit cell.[16−20] Although the highest temperature allowed by our experimental setup was 1373 K, we could not reach the $\delta \leftrightarrow \gamma$ phase transition, despite the slightly lower transition temperature of 1320−1348 K reported in earlier studies using differential thermal analysis (DTA) and X-ray diffraction.[17,20] The DTA data[17] demonstrate a significant hysteresis for the $\delta \leftrightarrow \gamma$ phase transition, the transition falls almost 50 K higher on heating than on cooling, and it is possible that in our experiments the transition temperature was not reached. Nevertheless, we consider δ-Sr_3WO_6 as the parent structure for other low temperature forms.

The γ-Sr_3WO_6 polymorph, stable below 1373 K, demonstrates a clear splitting of the perovskite subcell reflections which corresponds to a face-centered triclinic $2a_p \times 2a_p \times 2a_p$ subcell with two equal lattice parameters. This cell can be reduced to a body-centered monoclinic $\sqrt{2}a_p \times \sqrt{2}a_p \times 2a_p$ unit cell ($a_{s1} = 5.97834(3)$Å, $b_{s1} = 5.95793(3)$Å, $c_{s1} = 8.30725(4)$Å, $\beta = 90.2274(3)$Å at $T = 1173$ K). Numerous weaker reflections are present in the SXPD and NPD patterns of γ-Sr_3WO_6 indicating a superstructure which was analyzed by electron diffraction (Figure 2a−d). The brighter spots on the patterns ($T = 1073$ K) belong to the face-centered pseudo-cubic $2a_p \times 2a_p \times 2a_p$ subcell. Weaker reflections indicate a superstructure that can be indexed with a monoclinic unit cell with $a_m \approx 10.2$ Å, $b_m \approx 17.9$ Å, $c_m \approx 12.0$ Å, $\beta \approx 125°$. The relation between the unit cell vectors $\mathbf{a}_p$, $\mathbf{b}_p$, $\mathbf{c}_p$ of the parent $Fm\bar{3}m$ double perovskite structure and the monoclinic supercell is established as $\mathbf{a}_m = \mathbf{a}_p + 1/2\mathbf{b}_p - 1/2\mathbf{c}_p$, $\mathbf{b}_m = 3/2\mathbf{b}_p + 3/2\mathbf{c}_p$, $\mathbf{c}_m = -\mathbf{b}_p + \mathbf{c}_p$. The reflection conditions *hkl*: $h + k = 2n$, *h*0*l*: $h, l = 2n$ suggest $C2/c$ and Cc as possible space groups for γ-Sr_3WO_6.

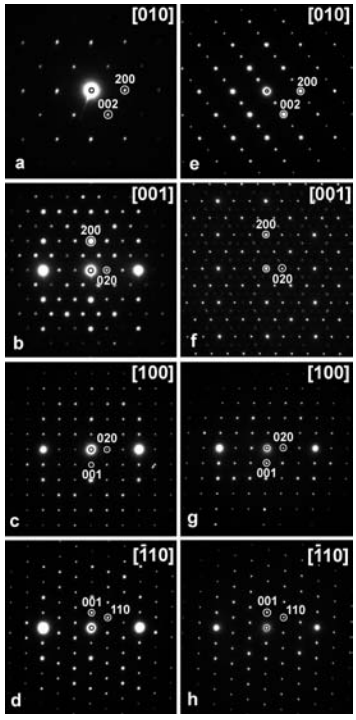

Figure 2. Electron diffraction patterns of Sr_3WO_6 at 1073 K (a−d) and at room temperature (e−h).

The β-Sr_3WO_6 polymorph, stable below 464−506 K, also shows the splitting of the subcell reflections, but the character of the splitting is different and consistent with the triclinically distorted $2a_p \times 2a_p \times 2a_p$ subcell with lattice parameters $a_{s2} = 8.22339(2)$Å, $b_{s2} = 8.30324(6)$Å, $c_{s2} = 8.36931(2)$Å, $\alpha = 90.2380(3)°$, $\beta = 89.7655(3)°$, $\gamma = 90.2770(3)°$ ($T = 300$ K). These subcell parameters are in agreement with the lattice parameters provided for Sr_3WO_6 by Kovba et al.[20] The room temperature ED patterns are similar to the ED patterns of the γ-Sr_3WO_6 polymorph, but demonstrate extra features (Figure 2e−h). All reciprocal lattice sections except the [001] ED pattern could be completely indexed with the *C*-centered unit cell (with slightly smaller lattice parameters because of thermal contraction) as for the γ-Sr_3WO_6 phase. However, deviation from monoclinic toward triclinic symmetry is obvious from the ED patterns. For example, clear deviation of α from 90° is visible on the [100] ED pattern (Figure 2g). At the same time, the *h*0*l*: $l \neq 2n$ reflections appear on the [010] ED pattern, indicating the absence of

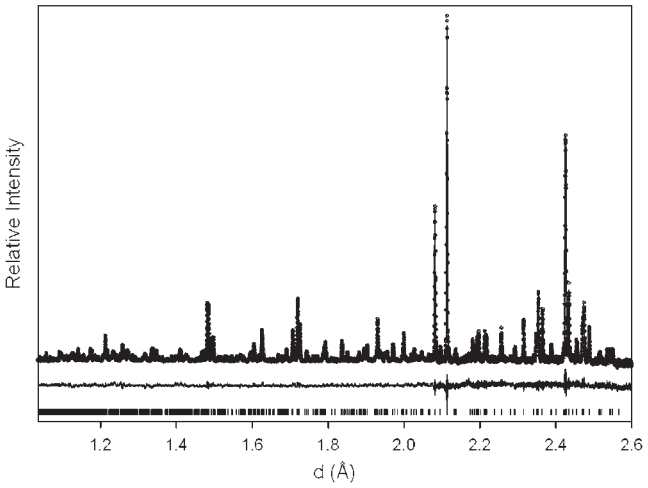

Figure 3. NPD pattern of γ-Sr_3WO_6 at 1373 K showing the observed (circles), calculated (solid line), difference (beneath), and *hkl* positions (tick marks).

a *c* glide plane. The reflections in the [001] ED pattern can be divided into two sets: the brighter sharp spots can be indexed with the *C*-centered triclinic supercell (we use the non-standard *C*1 setting for easy comparison with the γ-phase) with $a_{t1} \approx a_m$, $b_{t1} \approx b_m$, $c_{t1} \approx c_m$ whereas the weaker and more diffuse spots require a doubling of the *a* and *c* parameters. A new primitive triclinic unit cell with $a_{t2} \approx 20.2$ Å, $b_{t2} \approx 20.4$ Å, $c_{t2} \approx 11.8$ Å, $\alpha \approx 72.8°$, $\beta \approx 125.5°$, $\gamma \approx 120°$ and larger unit cell volume was constructed for a complete indexation of the patterns, related to the *C*-centered triclinic cell as $\mathbf{a}_{t2} = 2\mathbf{a}_{t1}$, $\mathbf{b}_{t2} = -\mathbf{a}_{t1} + \mathbf{b}_{t1}$, $\mathbf{c}_{t2} = \mathbf{c}_{t1}$. Thus, in comparison with the ED patterns of the γ-Sr_3WO_6 polymorph, two sets of extra reflections show up on the room temperature patterns, corresponding to propagation vectors $\mathbf{k}_1 = 0$ and $\mathbf{k}_2 = [1/2,0,1/2]$. On the basis of the SXPD and NPD results, we assume that the reflections corresponding to the $\mathbf{k}_1$ and $\mathbf{k}_2$ vectors are associated with two different polymorphs. The polymorph with the *C*-centered triclinic a_{t1}, b_{t1}, c_{t1} supercell will be further denoted as β-Sr_3WO_6, whereas the polymorph with the a_{t2}, b_{t2}, c_{t2} supercell will be denoted as α-Sr_3WO_6. Because of sensitivity of the superstructure to electron beam irradiation and uncontrolled heating introduced by the electron beam, no in situ observation of the phase transition between these polymorphs is possible.

The supercells derived from the ED patterns allowed the SXPD and NPD patterns to be indexed (Figures 1 and 3). The lattice parameters of the α, β, and γ phases at different temperatures are given in Supporting Information, Table S1. It should be mentioned that the SXPD pattern collected at RT can be indexed with a triclinic *C*-centered a_{t1}, b_{t1}, c_{t1} supercell and was attributed to the β-Sr_3WO_6 polymorph. The weak reflections corresponding to the triclinic primitive a_{t2}, b_{t2}, c_{t2} supercell of the α-Sr_3WO_6 polymorph were not observed on this pattern. However, these reflections are seen on the RT NPD pattern, which can be completely indexed only with the a_{t2}, b_{t2}, c_{t2} supercell ($a_{t2} = 20.1906(6)$Å, $b_{t2} = 20.3764(5)$Å, $c_{t2} = 11.8133(3)$Å, $\alpha = 72.887(2)°$, $\beta = 125.461(2)°$, $\gamma = 119.992(2)°$, Supporting Information, Figure S1). The fact that the $\alpha \leftrightarrow \beta$ transition did not occur at the SXPD measurements is thought to be related to the fast cooling of the thin capillary sample in comparison with the much larger sample used for the NPD experiments.

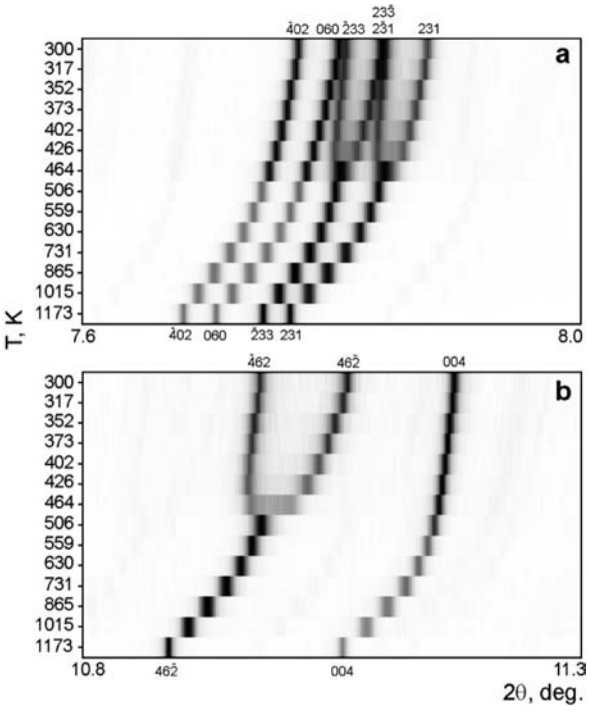

Figure 4. Splitting of the $2a_p \times 2a_p \times 2a_p$ subcell {220} (a) and {400} (b) reflections on going from the monoclinic γ-phase ($T = 1173$ K) to the triclinic β-phase ($T = 300$ K).

The $\gamma \leftrightarrow \beta$ phase transition was investigated in more detail. It manifests itself as a splitting of the reflections on going from the monoclinic to the triclinic symmetry. Figure 4 shows the splitting of the {220} and {400} perovskite $2a_p \times 2a_p \times 2a_p$ subcell reflections, indicating a transition temperature between 464 and 506 K, in good agreement with the transition temperature of 470 K, found from the temperature dependence of the dielectric permittivity.[17] The lattice parameters change monotonically with temperature without anomalies at the transition temperature (Figure 5, Supporting Information, Table S1). The β angle does not noticeably change above 900 K, but decreases almost linearly in the 900−300 K temperature range. The temperature dependence of the unit cell volume does not demonstrate a discontinuity at the transition temperature indicating a continuous $\gamma \leftrightarrow \beta$ phase transition. The *h*0*l*: $l \neq 2n$ reflections are present in the SXPD pattern of the β-Sr_3WO_6 phase; their intensity gradually vanishes up to complete disappearance above the phase transition point (Figure 6). Heating−cooling cycles and a good correspondence between the SXPD patterns of the β-Sr_3WO_6 phase before and after heating−cooling experiments indicate that the phase transition is reversible.

Although the reversible phase transition was well reproduced after several heating−cooling cycles, there were some differences in the thermal behavior of the diffraction patterns for the first heating ramp. A co-existence of the β-Sr_3WO_6 and γ-Sr_3WO_6 phases was observed in the SXPD pattern collected at 623 K as well as in the NPD patterns taken at 498, 798, and 898 K. In spite of its high complexity, the SXPD pattern at $T = 623$ K can be fitted

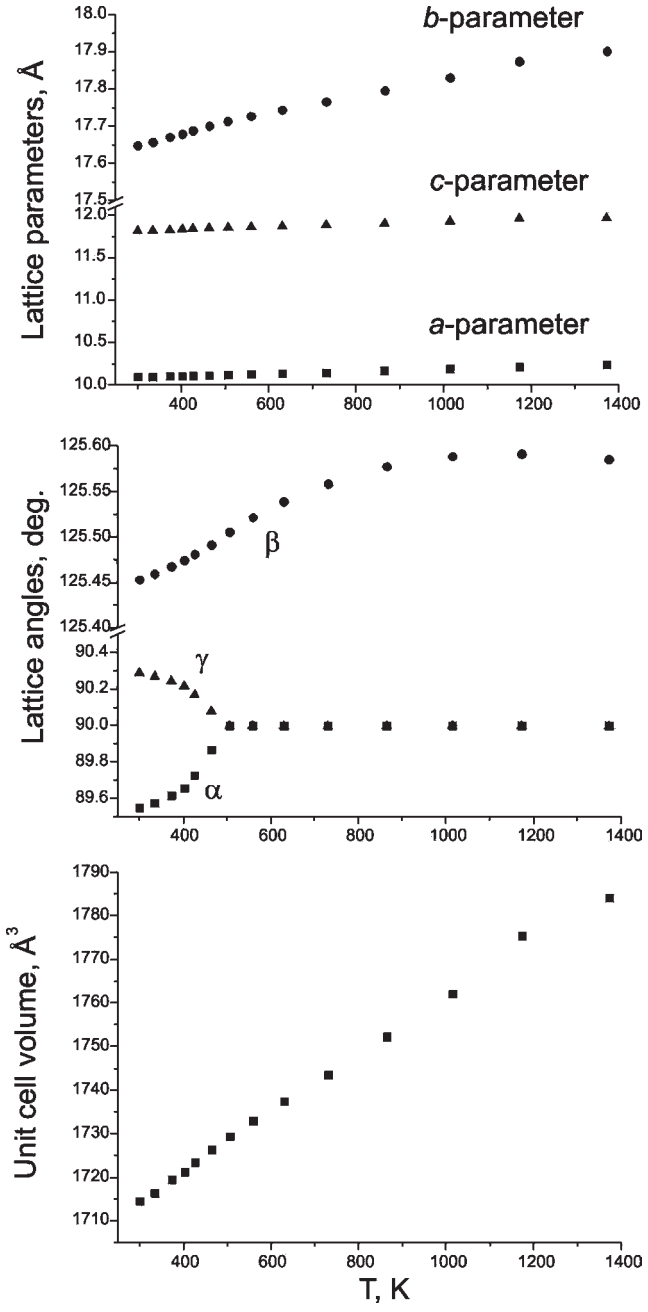

Figure 5. Temperature dependencies of the lattice parameters, lattice angles, and unit cell volume for Sr_3WO_6 in the 300−1373 K temperature range.

using the Le Bail method with subcell parameters a_{s2} = 8.2871(1)Å, b_{s2} = 8.2691(1)Å, c_{s2} = 8.3893(1)Å, α = 90.051(2)°, β = 89.741(2)°, γ = 90.250(1)° for the β-Sr_3WO_6 phase and a_{s1} = 5.93806(6)Å, b_{s1} = 5.91517(7)Å, c_{s1} = 8.24993(9)Å, β = 90.3311(7)° for the γ-Sr_3WO_6 phase (Supporting Information, Figure S2). Upon repeated heating and cooling cycles no co-existence of the β-Sr_3WO_6 and γ-Sr_3WO_6 phases is observed. One may assume that such behavior is not intrinsic to Sr_3WO_6 and is caused by the presence of some amount of water in the initial material, which is eliminated during the first heating cycle, so that the phase transition is combined with dehydration. This assumption is not unreasonable taking into account the high content of Sr in the compound and its sensitivity to air moisture, which results in a gradual decomposition of the material. Since the hydration/dehydration process is outside the scope of this article, this was not investigated in detail.

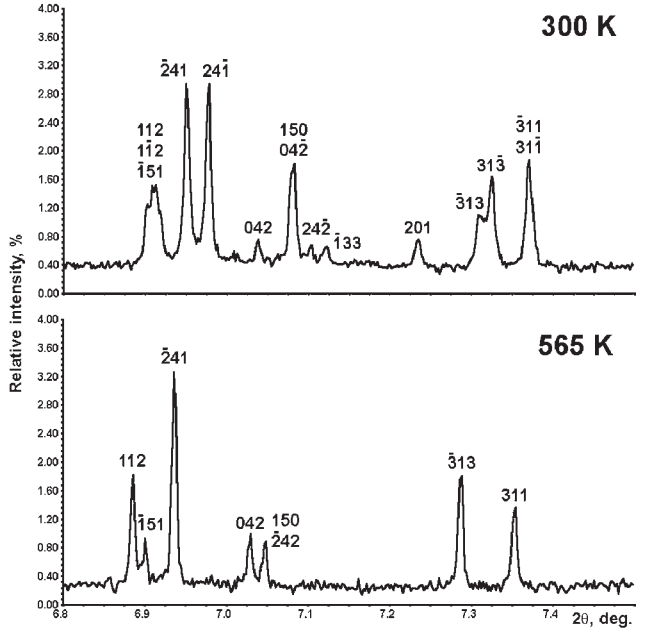

Figure 6. Part of the SXPD pattern of Sr_3WO_6 demonstrating a presence of the $h0l$, $l \neq 2n$ reflections for the β-phase (T = 300 K) and vanishing of these reflections for the γ-phase (T = 565 K).

3.2. Structure Determination. A complete crystal structure determination was carried out for the γ-Sr_3WO_6 and β-Sr_3WO_6 phases. Refinements of the γ-Sr_3WO_6 structure were attempted in space groups $C2/c$ and Cc. Despite extensive efforts, no good fits to the diffraction patterns could be obtained in $C2/c$ while excellent agreement was achieved using the non-centrosymmetric Cc space group. The unit cell volume of the γ-Sr_3WO_6 phase is three times that of the double perovskite parent cell and contains 120 atoms. There are no special positions in Cc and all atoms sit on 4-fold sites with three degrees of freedom. Therefore, there are 30 independent atoms and a total of 88 degrees of freedom for the atomic coordinates (two coordinates must be fixed to define the origin position in the ac plane). To reduce the number of variables during the initial steps of the refinements, rigid body approximations were used. It was assumed that the WO_6 octahedra remain as essentially rigid units while the coordination environment of the Sr atoms residing on the B-sites (hereafter denoted Sr_B) undergo a considerable change. Rigid oxygen octahedra were constructed around each of the three symmetrically independent W atoms with a W−O bond length of 1.93 Å. The starting positions for the cations were the positions they would occupy in the ideal double perovskite structure. The first stage of the refinement was carried out using the 1173 K SXPD pattern to locate the approximate positions of the cations. Next, the rotation angles of the oxygen octahedra were found using the 1373 K NPD pattern by a global optimization with a simulated annealing algorithm. Next, the rigid body restraints were removed, soft distance constraints were introduced, and all atoms were refined using both the SXRD and the NPD patterns. Once the atom

Table 1. Selected Parameters from the Rietveld Refinements for Sr_3WO_6

phase	γ-Sr_3WO_6	β-Sr_3WO_6
space group	*Cc*	*C*1
T (K)	1373	300
a (Å)	10.2363(1)	10.09496(3)
b (Å)	17.9007(1)	17.64748(5)
c (Å)	11.9717(1)	11.81400(3)
α (deg)	90	89.5470(2)
β (deg)	125.585(1)	125.4529(2)
γ (deg)	90	90.2889(2)
Z	12	12
cell volume ($Å^3$)	1784.01(1)	1714.40(1)
calculated density (g/cm^3)	6.062	6.306
radiation	neutron TOF	synchrotron X-ray, $\lambda = 0.39998$ Å
d range (Å)	1.1−2.6	0.669−8.000
parameters refined	92	176
R_I, R_P, R_{wP}	0.009, 0.026, 0.037	0.018, 0.075, 0.103

locations were essentially solved, the atomic displacement parameters (ADPs) were refined. All atoms corresponding to the same element were restricted to have the same ADP to reduce the number of variables. Finally, refinements were done against either the 1173 K SXPD pattern or the 1373 K NPD pattern to verify the structure using both diffraction techniques. For the refinement from SXPD data the Sr_2WO_5 admixture was taken into account (weight fraction of 2.4%). The final fits (Figures 1 and 3) are characterized by $R_I = 0.009$, $R_P = 0.026$, $R_{wP} = 0.037$ for the NPD pattern and $R_I = 0.030$, $R_P = 0.062$, $R_{wP} = 0.085$ for the SXPD pattern. All further discussion of the γ-Sr_3WO_6 structure is based on the 1373 K coordinates, although it should be noted that the structure at 1173 K is nearly indistinguishable.

The relative intensity of the $h0l$: $l \neq 2n$ reflections arising because of loss of the *c* glide plane upon the $\gamma \rightarrow \beta$ phase transition does not exceed 0.4% of the most intense peak in the pattern, indicating that the structural changes at this phase transition are very subtle. The initial model of the β-Sr_3WO_6 structure was derived by a transformation of the γ-Sr_3WO_6 structure from the *Cc* to the *C*1 space group. The refinement was performed with soft constraints on the Sr−O distances and common ADPs for all atoms. The refinement from the SXPD data readily converged to $R_I = 0.018$, $R_P = 0.075$, $R_{wP} = 0.103$. Because of the very large number of refined parameters, this structure can only be considered approximate.

The crystallographic data for the β- and γ-phases are summarized in Table 1. The selected interatomic distances for the γ-phase are listed in Table 2. The interatomic distances for the β-phase are listed in Supporting Information, Table S2. The atomic coordinates of the β- and γ-phases are provided in the Supporting Information, Tables S3 and S4, respectively.

The α-Sr_3WO_6 phase has a unit cell volume double that of the β-Sr_3WO_6 phase and lower symmetry. The huge number of degrees of freedom for the atom positions coupled with pathological reflection overlap on the NPD pattern prevented us from solving this structure from powder diffraction data.

3.3. Structural Description of β- and γ-Polymorphs. The crystal structures of the β- and γ-polymorphs of Sr_3WO_6 can be described, to a first approximation, as derivatives of the double perovskite structure where 1/3 of the WO_6 octahedra have been rotated by ~45°. The relationship between the double perovskite pseudo-cubic

Table 2. Selected Interatomic Distances for γ-Sr_3WO_6 (Å)

W Cations					
W(1)−O(1)	1.87(1)	W(2)−O(18)	1.90(2)	W(3)−O(17)	1.85(2)
W(1)−O(2)	1.88(2)	W(2)−O(14)	1.91(2)	W(3)−O(8)	1.86(2)
W(1)−O(6)	1.91(2)	W(2)−O(10)	1.93(2)	W(3)−O(9)	1.87(2)
W(1)−O(4)	1.93(2)	W(2)−O(7)	1.96(3)	W(3)−O(11)	1.89(2)
W(1)−O(3)	1.97(2)	W(2)−O(16)	1.96(2)	W(3)−O(13)	1.96(2)
W(1)−O(5)	1.99(2)	W(2)−O(15)	1.99(3)	W(3)−O(12)	1.99(2)
Sr_B Cations					
Sr(1)−O(9)	2.41(1)	Sr(2)−O(3)	2.42(1)	Sr(3)−O(11)	2.42(1)
Sr(1)−O(2)	2.41(1)	Sr(2)−O(13)	2.45(1)	Sr(3)−O(6)	2.44(1)
Sr(1)−O(1)	2.42(1)	Sr(2)−O(18)	2.45(1)	Sr(3)−O(5)	2.57(1)
Sr(1)−O(8)	2.43(1)	Sr(2)−O(4)	2.45(2)	Sr(3)−O(17)	2.64(1)
Sr(1)−O(15)	2.70(1)	Sr(2)−O(15)	2.67(1)	Sr(3)−O(16)	2.68(1)
Sr(1)−O(14)	2.76(1)	Sr(2)−O(16)	2.69(1)	Sr(3)−O(14)	2.81(1)
Sr(1)−O(7)	2.78(2)	Sr(2)−O(12)	2.69(1)	Sr(3)−O(10)	2.85(1)
				Sr(3)−O(10)	3.02(1)
Sr_A Cations					
Sr(4)		Sr(5)		Sr(6)	
Sr(4)−O(16)	2.54(1)	Sr(5)−O(15)	2.48(1)	Sr(6)−O(14)	2.60(1)
Sr(4)−O(10)	2.54(1)	Sr(5)−O(1)	2.52(1)	Sr(6)−O(2)	2.65(2)
Sr(4)−O(11)	2.56(2)	Sr(5)−O(8)	2.63(1)	Sr(6)−O(5)	2.73(2)
Sr(4)−O(6)	2.72(1)	Sr(5)−O(3)	2.75(1)	Sr(6)−O(3)	2.75(2)
Sr(4)−O(8)	2.85(2)	Sr(5)−O(17)	2.89(1)	Sr(6)−O(4)	2.77(1)
Sr(4)−O(7)	2.86(1)	Sr(5)−O(5)	2.89(1)	Sr(6)−O(8)	2.86(2)
Sr(4)−O(1)	2.87(1)	Sr(5)−O(4)	2.15(2)	Sr(6)−O(12)	2.87(1)
Sr(4)−O(17)	2.89(2)	Sr(5)−O(6)	2.15(1)	Sr(6)−O(7)	2.93(1)
Sr(4)−O(3)	3.03(2)	Sr(5)−O(7)	2.17(2)		
Sr(7)		Sr(8)		Sr(9)	
Sr(7)−O(16)	2.49(1)	Sr(8)−O(13)	2.55(1)	Sr(9)−O(11)	2.54(1)
Sr(7)−O(18)	2.60(1)	Sr(8)−O(15)	2.63(2)	Sr(9)−O(13)	2.57(2)
Sr(7)−O(9)	2.66(1)	Sr(8)−O(9)	2.68(1)	Sr(9)−O(10)	2.68(2)
Sr(7)−O(14)	2.70(1)	Sr(8)−O(12)	2.79(2)	Sr(9)−O(12)	2.68(2)
Sr(7)−O(2)	2.71(1)	Sr(8)−O(18)	2.79(2)	Sr(9)−O(4)	2.72(2)
Sr(7)−O(6)	2.73(1)	Sr(8)−O(17)	2.80(2)	Sr(9)−O(5)	2.89(1)
Sr(7)−O(3)	2.76(1)	Sr(8)−O(1)	3.04(2)	Sr(9)−O(7)	2.90(2)
Sr(7)−O(12)	2.85(2)	Sr(8)−O(11)	3.16(2)	Sr(9)−O(17)	3.07(2)
		Sr(8)−O(5)	3.16(2)	Sr(9)−O(2)	3.17(1)

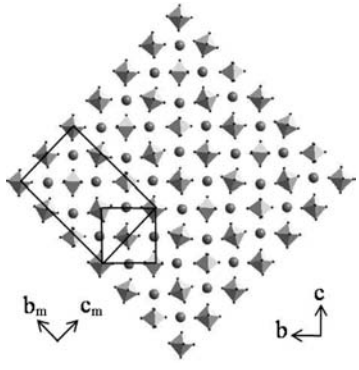

Figure 7. Relationship between the double perovskite pseudo-cubic $a \approx b \approx c \approx 2a_p$ subcell and the monoclinic a_m, b_m, c_m supercell of γ-Sr_3WO_6 in the *bc*-plane. One layer of WO_6 ocathedra and Sr_B cations (spheres) is shown. The square box shows one double perovskite unit cell, and the rectangular box shows the unit cell of γ-Sr_3WO_6.

$a \approx b \approx c \approx 2a_p$ subcell and the monoclinic a_m, b_m, c_m supercell of γ-Sr_3WO_6 is shown in Figure 7. The crystal structure of γ-Sr_3WO_6 is shown in Figure 8. There are three symmetrically unique W atoms in the unit cell surrounded by oxygen octahedra. The orientations of 2/3 of the WO_6 octahedra are close to what they would be in the ideal double perovskite structure, while the orientation of the remaining 1/3 of the WO_6 octahedra are drastically altered. The W(1)O_6 octahedron is slightly distorted but

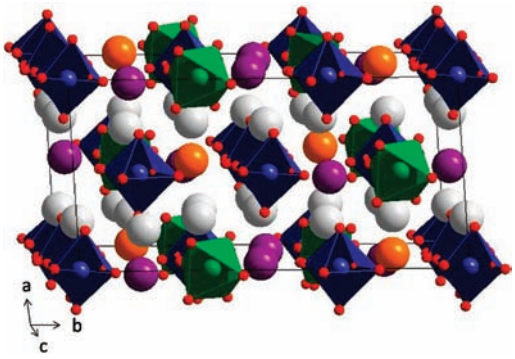

Figure 8. Crystal structure of γ-Sr_3WO_6. The blue octahedra are the WO_6 polyhedra which are only subtly distorted from their ideal positions while the green octahedra are the WO_6 units which are rotated by ~45°. The blue or green central atoms are the W atoms, and the small red spheres are the oxygen atoms. The purple spheres are the 7-coordinated Sr_B atoms, the orange spheres are the 8-coordinated Sr_B atoms, and the gray spheres are the Sr_A atoms.

is essentially untilted, keeping the same orientation as in the parent double perovskite structure. The octahedron surrounding the W(3) atom is more symmetric but is rotated by roughly 16° about the *a*-axis of the subcell. The octahedron surrounding the W(2) atom is rotated by ~45° relative to the double perovskite structure. The rotations of these octahedra are related by symmetry such that half of the $W(2)O_6$ octahedra are rotated about the *c* subcell axis and half are rotated about the *b* subcell axis with equal rotation angles. The structure can most easily be visualized as two layers of WO_6 octahedra and Sr_B cations with the Sr_A cations lying between the layers, as shown in Figure 9. The layers alternate along the a_m axis. The pattern of rotated octahedra in every layer can be described by the matrix

$$\begin{pmatrix} 0 & b & a \\ 0 & a & c \end{pmatrix}$$

where the rows correspond to the b_m direction, columns correspond to the $\boldsymbol{c}_m$ direction, and 0, ***a***, ***b***, ***c*** stand for the untilted octahedra and the octahedra rotated about the *a*, *b*, and *c* subcell axes, respectively. In the adjacent layers along the a_m axis the tilting pattern is shifted by the [0,1/2,0] vector. The bond valence sums of the W(1), W(2), and W(3) atoms are 5.94, 5.64, and 6.28, respectively, in good agreement with their nominal valence of 6.

In the ideal double perovskite structure each BO_6 octahedron shares a corner with each of the six surrounding $B'O_6$ octahedra. The 45° rotations of the WO_6 octahedra in Sr_3WO_6 break the corner sharing connectivity between the WO_6 octahedra and four out of six neighboring Sr_B polyhedra. The two Sr_B atoms that lie along the rotation axis are unaffected by this rotation. The coordination polyhedra of the four Sr_B atoms that lie in the plane perpendicular to the axis of rotation now share an edge with the rotated WO_6 octahedron and their coordination number is increased by one for each edge sharing neighbor. In Sr_3WO_6 the octahedral rotations are such that 2/3 of the Sr_B cations have a 7-fold coordination geometry while the other 1/3 become 8-fold coordinated. The Sr_B cations now form highly elongated bonds to the two oxygen atoms on the rotated WO_6 octahedra. As a result the Sr_B atoms undergo significant shifts from their ideal positions toward the WO_6 octahedra with which they share an edge. The Sr(1) and Sr(2) atoms are each shifted ~0.5 Å toward the WO_6 octahedra with which they share an edge. This results in an asymmetrical coordination environment consisting of 4 short and 3 long bonds (Table 2). The bond valences of the Sr(1) and Sr(2) atoms are calculated to be 2.34 and 2.31, respectively, indicating that they are somewhat overbonded. The coordination polyhedron of the Sr(3) atom shares edges with two WO_6 octahedra located at *cis*-positions with respect to each other giving a coordination number of 8. It is shifted ~0.5 Å along the diagonal direction between these two WO_6 octahedra. The coordination environments of the Sr_B atoms are shown in Figure 10. The bond valence of the Sr(3) atom is 2.00 indicating that it has obtained an ideal bonding environment. The octahedral tilting also changes the coordination environments of the Sr_A atoms. Their coordination numbers are effectively reduced from 12 to either 9 or 8. Bond valence sums for the Sr_A atoms range from 1.44 to 1.79, indicating that they are still somewhat under-bonded despite the large octahedral rotations. Nevertheless, we should keep in mind that the ideal lengths of the rather ionic Sr−O bonds will increase as temperature rises, yet the bond valence parameters used for these calculations were derived from room temperature structures. Hence the ideal bond valence sum for strontium is probably less than 2.

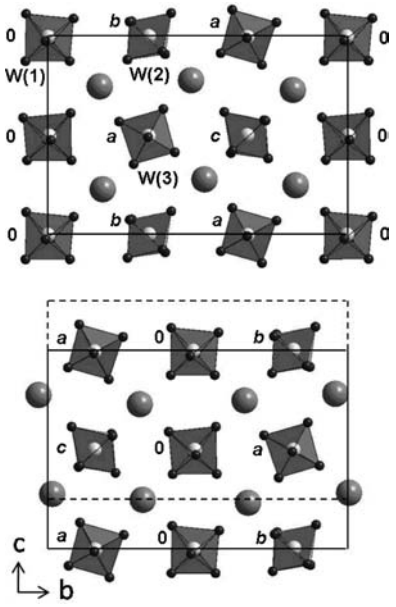

Figure 9. Two layers alternating along the a_m axis in the γ-Sr_3WO_6 structure. The small light gray spheres are W, small black spheres are O, and the large gray spheres are Sr_B. The dotted lines in the bottom figure show the projection of the layer beneath when looking down the direction perpendicular to the image plane. The tilting notations are assigned to every octahedron.

The crystal structure of the β-Sr_3WO_6 phase does not differ drastically from that of the γ-Sr_3WO_6 phase. In γ-Sr_3WO_6 the *c* glide plane makes identical octahedral tilt angles about the *b* and *c* perovskite subcell axes (i.e., for the ***b*** and ***c*** types of the WO_6 octahedra). The transition to the β-Sr_3WO_6 phase with triclinic symmetry removes this symmetry restriction allowing different rotation angles for the ***b*** and ***c*** octahedra (Figure 11). At the same time the

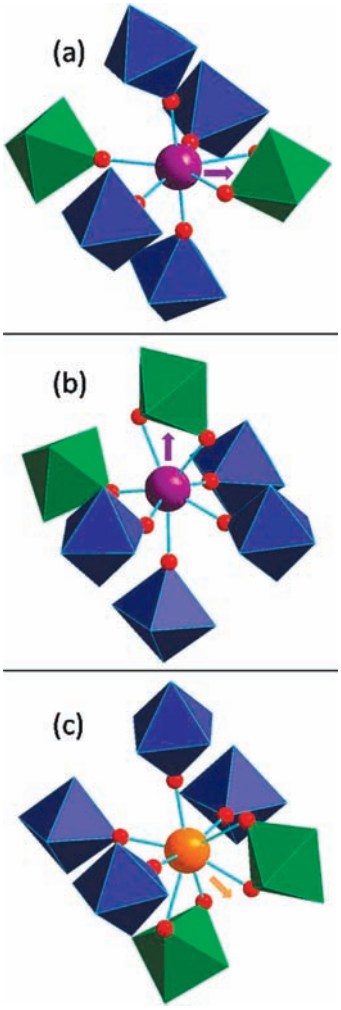

Figure 10. Coordination environments of the Sr(1) (a), Sr(2) (b), and Sr(3) (c) atoms. The color scheme is the same as in Figure 8. The arrows show the directions of the Sr displacements.

$\gamma \rightarrow \beta$ phase transition is accompanied by a noticeable increase of the distortion of the WO_6 octahedra (Supporting Information, Table S2). The average value of the octahedral distortion parameter $\Delta d = (1/6)\sum_{n=1-6}[(d_n - d)/d]^2$ (d_n are the individual W−O distances and d is the average ⟨W−O⟩ distance[24]) increases from 5.17×10^{-4} in γ-Sr_3WO_6 to 1.58×10^{-3} in β-Sr_3WO_6.

4. Conclusions

The crystal structure of Sr_3WO_6 is a representative of the double perovskites with a broken corner sharing connectivity of the octahedral framework. It confirms the recently formulated criteria which have to be fulfilled to stabilize such type of perovskite structure with non-cooperative octahedral rotations: a size difference between the B and B' cations of

(24) Alonso, J. A.; Martinez-Lopez, M. J.; Casais, M. T.; Fernandez-Diaz, M. T. *Inorg. Chem.* **2000**, *39*, 917–923.

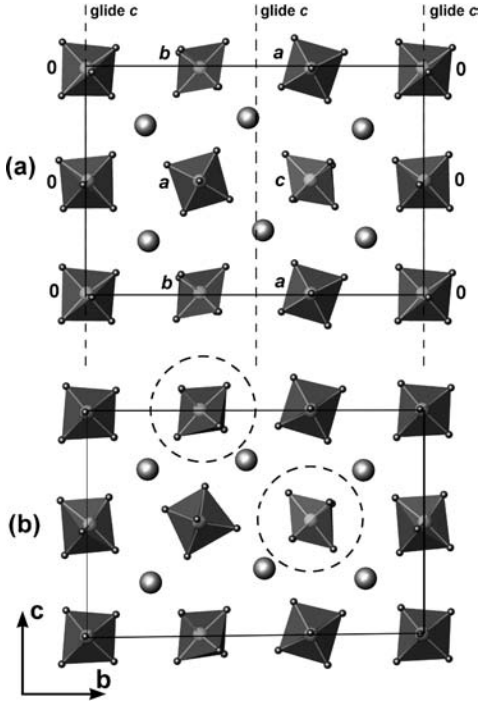

Figure 11. Comparison of two layers in the *bc*-plane of the γ-Sr_3WO_6 (a) and β-Sr_3WO_6 (b) structures. The *c* glide plane in γ-Sr_3WO_6 is marked with vertical dashed lines. The ***b*** and ***c*** octahedra with equal tilt amplitudes due to the *c* glide plane in γ-Sr_3WO_6 acquire slightly different tilt angles in β-Sr_3WO_6 with triclinic symmetry.

$\Delta IR = 0.50-0.66$ Å ($\Delta IR = 0.58$ Å for Sr_3WO_6) and a reasonably small tolerance factor $t = 0.89-0.93$ ($t = 0.89$ for Sr_3WO_6). The arrangement of the rotated WO_6 octahedra around the Sr_B cations is also in agreement with the energetically favorable rotation modes. Increasing the coordination number of the Sr_B cations occurs either by ~45° rotation of a single WO_6 octahedron or by rotation of two WO_6 octahedra in *cis*-positions about two non-coplanar perpendicular axes. These rotation modes correspond to minimal electrostatic repulsion between the oxygen atoms and allow relaxation of the Sr_B−O bonds because of displacements of the Sr_B cations from their ideal perovskite positions.

Acknowledgment. This work was supported by the Russian Foundation of Basic Research (RFBR Grant 06-03-90168-a). G.K. and P.M.W. acknowledge financial support from the National Science Foundation (Award number DMR-0907356). A.M.A. acknowledges the European Synchrotron Radiation Facility for provision of synchrotron radiation facilities and thanks Andy Fitch for assistance in using beamline ID31. G.K. and P.M.W. would like to thank Aziz Daoud-Aladine and Kevin Knight for assistance in collecting the NPD data.

Supporting Information Available: Figures S1 and S2 and Tables S1−S4. This material is available free of charge via the Internet at http://pubs.acs.org.